

Topological Defects and Interactions in Nematic Emulsions

T.C. Lubensky, David Pettey, and Nathan Currier

Department of Physics and Astronomy, University of Pennsylvania, Philadelphia, PA 19104, USA

Holger Stark

Institut für Theoretische und Angewandte Physik, Universität Stuttgart, D-70550 Stuttgart, Germany

Inverse nematic emulsions in which surfactant-coated water droplets are dispersed in a nematic host fluid have distinctive properties that set them apart from dispersions of two isotropic fluids or of nematic droplets in an isotropic fluid. We present a comprehensive theoretical study of the distortions produced in the nematic host by the dispersed droplets and of solvent mediated dipolar interactions between droplets that lead to their experimentally observed chaining. A single droplet in a nematic host acts like a macroscopic hedgehog defect. Global boundary conditions force the nucleation of compensating topological defects in the nematic host. Using variational techniques, we show that in the lowest energy configuration, a single water droplet draws a single hedgehog out of the nematic host to form a tightly bound dipole. Configurations in which the water droplet is encircled by a disclination ring have higher energy. The droplet-dipole induces distortions in the nematic host that lead to an effective dipole-dipole interaction between droplets and hence to chaining.

PACS numbers: 77.84.Nh, 61.30.Cz, 61.30.Jf

I. INTRODUCTION

Topological defects [1–4], which are a necessary consequence of broken continuous symmetry, exist in systems as disparate as superfluid helium 3 [5] and 4 [6], crystalline solids [7–9], liquid crystals [10,11], and quantum-Hall fluids [12]. They play an important if not determining role in such phenomena as response to external stresses [8,9], the nature of phase transitions [4,13,14], or the approach to equilibrium after a quench into an ordered phase [15]; and they are the primary ingredient in such phases of matter as the Abrikosov flux-lattice phase of superconductors [16,17] or the twist-grain-boundary phase of liquid crystals [18–20]. They even arise in certain cosmological models [21]. Given the universal nature of topological defects, it is always interesting to find new systems that allow us to increase our understanding of these defects. In this paper, we will present a detailed theoretical investigation of a new class of nematic emulsions [22] whose intriguing properties are controlled by a class of topological defects called hedgehogs. These emulsions are either simple inverse emulsions in which surfactant-coated water droplets are dispersed in an aligned nematic host, or they are multiple emulsions in which water droplets are dispersed in larger nematic drops that in turn are dispersed in water.

Liquid crystals are ideal materials for studying topological defects. Distortions yielding defects are easily produced through control of boundary conditions, surface geometries, and external fields. The resulting defects are easily imaged optically. The many different liquid crystalline phases (nematic, cholesteric, smectic-*A*, smectic-*C*, etc.) with different symmetry ground states make it possible to study different kinds of defects. Over the

years, liquid crystals have provided us with detailed and visually striking information about topological defects.

Liquid crystal emulsions in which surfactant-coated drops containing a liquid-crystalline material are dispersed in water have been a particularly fruitful medium for studying topological defects [23–26,10]. The liquid-crystalline drops are typically from $10\mu\text{m}$ to $50\mu\text{m}$ in diameter and are visible under a microscope. Changes in alignment direction, specified by the Frank director \mathbf{n} , are easily studied under crossed polarizers. The isolated drops in these emulsions provide an idealized spherical confining geometry for the liquid crystal. More general distorted or multiply connected random geometries [26] such as those produced in polymer-dispersed liquid crystals (PDLCs) [27,28], in emulsion films, or in dispersions of agglomerations of silica spheres in a nematic host [29] are of considerable current interest because of display technologies based upon changing the light scattering properties of these systems through modification of defect distributions via external fields.

In this paper, we will study inverse and multiple nematic emulsions. These emulsions differ from the direct emulsions described above in that isotropic water droplets are dispersed in a nematic host rather than the other way around. They are considerably more complex than direct emulsions. In direct emulsions, the nematic is separated into distinct, nearly spherical drops. Normal or homeotropic boundary conditions on the nematic director at a drop's surface will lead to a single point hedgehog defect in its interior; tangential boundary conditions will lead to a pair of surface defects called boojums [30,25,31]. Though there can be transitions among various director configurations as temperature or boundary conditions are changed [32,33], the topological structure of these drops

is simple. In inverse emulsions, each water drop with homeotropic boundary conditions will create a hedgehog director configuration in its immediate vicinity. Global boundary conditions at the surface of the nematic restrict total topological charge. Thus, in order to satisfy global constraints, additional defects must be created out of the nematic to compensate for or to cancel the topological charge created by droplets. The nature and placement of these additional defects determine the far-field director distortion produced by a droplet and the nature of droplet-droplet interactions. Experiments [22,34] show that each water droplet creates a companion point defect leading to dipole distortions of the director field at large distances. This is in contrast to the quadrupolar “Saturn-ring” configuration in which a disclination ring encircles a droplet at its equator that has been extensively studied [35–38]. Our calculations show that the experimentally observed dipole configuration is the preferred one and that it leads to a dipole-dipole interaction between drops that gives rise to the experimentally observed chaining of droplets. It is interesting to note that similar topological dipole configurations appear in two-dimensional systems including (1) free standing smectic films [39] where a circular region with an extra layer plays the role of the emulsion water droplet and (2) Langmuir films [40] in which a liquid-expanded inclusion in a tilted liquid-condensed region plays a similar role.

The outline of this paper is as follows. In Sec. II, we review important elastic and topological properties of nematics. In Sec. III, we provide an overview of important experimentally observed properties of inverse and multiple nematic emulsions. In Sec. IV, we calculate the director configurations and energy of a single water droplet in a uniform nematic using various variational ansatzes. In Sec. V, we introduce a phenomenological free energy to describe long-distance director distortions and interactions among droplets. Finally, In Sec. VI, we summarize our results.

II. ORDER, ENERGY, AND TOPOLOGICAL DEFECTS IN NEMATICS

A nematic liquid crystal is a uniaxial, homogeneous fluid characterized by a unit vector \mathbf{n} , called the Frank director, specifying the direction of the principal axis of a symmetric-traceless-tensor order parameter. The ground-state free energy of a nematic is invariant under all spatially uniform rotations of \mathbf{n} and under all inversions $\mathbf{n} \rightarrow -\mathbf{n}$. In addition, all physically observable quantities are invariant under $\mathbf{n} \rightarrow -\mathbf{n}$. The ground-state manifold or order-parameter space is the unit sphere in three dimensions S^2 with opposite points identified, i.e., the projective plane $RP^2 = S^2/Z_2$ [2,3,10]. The topological structure of the ground-state manifold determines the types of possible topological defects. As we will review below, nematics can have both line defects (disclinations) and point defects (hedgehogs).

A. The Frank Free Energy

The energy of slowly varying spatial distortions of the director $\mathbf{n}(\mathbf{r})$ is determined by the Frank free energy

$$F = \frac{1}{2} \int d^3r \{ K_1(\nabla \cdot \mathbf{n})^2 + K_2(\mathbf{n} \cdot \nabla \times \mathbf{n})^2 + K_3[\mathbf{n} \times (\nabla \times \mathbf{n})]^2 \} - \int d^3r K_{24} \nabla \cdot [\mathbf{n} \times (\nabla \times \mathbf{n}) + \mathbf{n}(\nabla \cdot \mathbf{n})], \quad (1)$$

where K_1 , K_2 , K_3 , and K_{24} are, respectively, the splay, twist, bend, and saddle-splay elastic constants. (There is also the possibility of another surface term with energy $K_{13}\nabla \cdot (\mathbf{n}\nabla \cdot \mathbf{n})$ [41,42], which we will not consider in this paper.) The saddle splay term is a pure divergence; it reduces to integrals over all surfaces, including interior surfaces formed, for example, by water droplets. For spherical surfaces with normal boundary conditions, these integrals are constant and do not vary, for example, when separations between droplets are changed. To keep our calculations as simple as possible, we will use the one-constant limit of the Frank free energy:

$$F = \frac{1}{2}K \int d^3r [(\nabla \cdot \mathbf{n})^2 + (\nabla \times \mathbf{n})^2] \quad (2)$$

$$-K_{24} \int d\mathbf{S} \cdot [\mathbf{n}\nabla \cdot \mathbf{n} + \mathbf{n} \times (\nabla \times \mathbf{n})] = \frac{1}{2}K \int d^3r \nabla_i n_j \nabla_i n_j + \frac{1}{2}(K - 2K_{24}) \int d\mathbf{S} \cdot [\mathbf{n}\nabla \cdot \mathbf{n} + \mathbf{n} \times (\nabla \times \mathbf{n})]. \quad (3)$$

Since surface energies do not play an important role in the phenomena to be discussed in the paper, we will set the saddle-splay constant K_{24} equal to zero unless otherwise specified. When $K = 2K_{24}$, the free energy reduces to the first line of Eq. (3), which is invariant with respect to rigid rotations of any director configuration. [Note: In Ref. [22], calculations were done with $K = K_{24}$.]

B. Surface Energies

Surfaces generally impose a preferred alignment direction of the nematic director relative to their local normals. The energetics of this alignment are described by the Rapini-Papouliar phenomenological surface free energy [43]

$$F_S = \frac{1}{2}W \int dS \sin^2 \gamma \quad (4)$$

where γ is the angle between the director and the surface normal. Homeotropic or normal alignment is favored by $W > 0$ and tangential alignment by $W < 0$. The coupling constant W varies in the range $10^{-4}\text{--}1 \text{ erg/cm}^2$ [44] with typical values of order 10^{-3} erg/cm^2 [45].

In addition to the above surface alignment energy, in emulsions, there is the energy arising from the surface tension of the water-surfactant-oil interface. This energy is simply the surface tension σ times the total surface area

$$F_\sigma = \sigma \int dS. \quad (5)$$

The surface tension is of order 10 erg/cm^2 [46].

We can now discuss the relative importance of the surface energies and the bulk Frank energy. Consider a spherical nematic drop of radius a with $W > 0$. If the director is everywhere normal to the surface, as the surface alignment energy favors, the Frank elastic energy is $8\pi K a$, and the surface alignment energy is zero. On the other hand, if the director is parallel throughout the interior of the drop, the Frank energy is zero, and the surface alignment energy is $8\pi W a^2/3$. The surface energy scales as a^2 , whereas the elastic energy scales as a . Thus, surface energy dominates over elastic energy for large drops, and we may assume, to a good approximation, that the preferred direction of surface alignment is imposed as a constraint. On the other hand for small droplets, elastic energy dominates over surface energy, and we should expect the surface director to deviate from its preferred orientation. The characteristic droplet dimension beyond which we may assume rigid boundary conditions is $r_c = K/W \approx 10^{-6}/3 \times 10^{-2} \approx 0.3 \mu\text{m}$. Typical droplet radii in the experiments of Poulin *et al.* [22] are larger than $1 \mu\text{m}$, and we may use rigid boundary conditions to interpret them.

Similar considerations apply to shape distortions of the droplets. The positive surface tension favors spherical drops of either liquid crystal in water or of water in liquid crystal. The surface energy scales as σa^2 . Thus, we can expect drops to be spherical and undistorted by the nematic director for drops larger than $r_\sigma = K/\sigma \approx 1 \text{ nm}$. In what follows, we will assume that water droplets remain spherical and that normal boundary conditions are rigidly imposed at nematic-water interfaces.

C. Topological Defects

Topological defects in ordered media are singular regions of spatial dimension less than that of physical space that are surrounded by order-parameter configurations that cannot be transformed to a homogeneous ground state via continuous deformations. There are two kinds of topological defects in a nematic. They are (1) line defects, called disclinations, with winding number of strength $1/2$ in which the director undergoes a rotation of π in one circuit around any one-dimensional path encircling the linear defect core, and (2) point defects, called hedgehogs, in which the director sweeps out all directions on the unit sphere S^2 as all points on any two-dimensional surface enclosing the defect core are visited.

The only topologically stable disclinations have winding number $1/2$. All director configurations on a loop can either be shrunk continuously to a single point in the order parameter space, in which case the loop encloses no defect, or they can be continuously distorted to a path in RP^2 starting at some arbitrary point and ending at a diametrically opposite point, in which case the loop, encloses a disclination of strength $1/2$. Typical director configurations for a strength $1/2$ disclination are shown in Fig. 1.

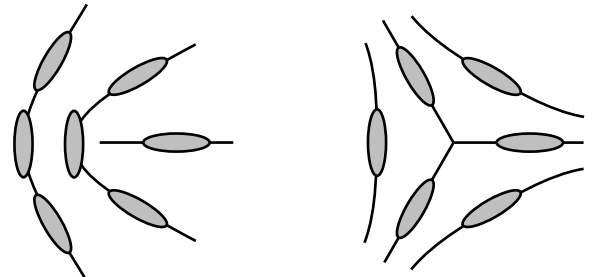


FIG. 1. Two director configurations for a strength $1/2$ disclination. In a two-dimensional nematic, the left and right figures correspond, respectively, to disclinations of strength $+1/2$ and $-1/2$. In a three-dimensional nematic, these configurations can be converted into each other via continuous transformations of the director

In the simplest disclination configurations shown in Fig. 1, the director is $\mathbf{n} = (\cos \phi/2, \pm \sin \phi/2, 0)$, where $\phi = \tan^{-1} y/x$ is the azimuthal angle in the xy -plane. The energy per unit length of such disclination lines calculated from Eq. (2) is

$$\epsilon = \frac{1}{4} \pi K \ln(R/r_c) + \epsilon_c, \quad (6)$$

where R is the sample radius, r_c is the radius of the disclination core, and ϵ_c is the core energy per unit length, which is of order K .

Hedgehogs are point defects characterized by an integer topological charge q specifying the number of times the unit sphere is wrapped by the director on any surface enclosing the defect core. An analytical expression for q is [3]

$$q = \frac{1}{8\pi} \int dS_i \epsilon_{ijk} \mathbf{n} \cdot (\partial_j \mathbf{n} \times \partial_k \mathbf{n}), \quad (7)$$

where the integral is over any surface enclosing the defect core. For an order parameter with O_3 (vector) symmetry, the order-parameter space is S^2 , and hedgehogs can have positive or negative charges. Nematic inversion symmetry makes positive and negative charges equivalent, and we may, as a result, take all charges to be positive.

There is a continuous infinity of director configurations for each value of the hedgehog charge. In the simplest unit-charge hedgehog configuration shown in Fig. 2(a), the director points radially outward from the point core like the electric field near a point charge. This configuration is called a *radial* hedgehog for obvious reasons.

Other configurations can be obtained from the radial configuration via rotations through arbitrary angles about any axis. Two examples are shown in Figs. 2(b) and (c). When the director of a radial hedgehog is rotated about a fixed axis through π , a *hyperbolic* hedgehog shown in Fig. 2(c) is produced. The hyperbolic hedgehog can be obtained from a radial hedgehog via a series of continuous distortions of the director passing through intermediate configurations such as the “circular” configuration shown in Fig. 2 (b). Thus, radial, hyperbolic, and all intermediate hedgehogs are topologically equivalent.

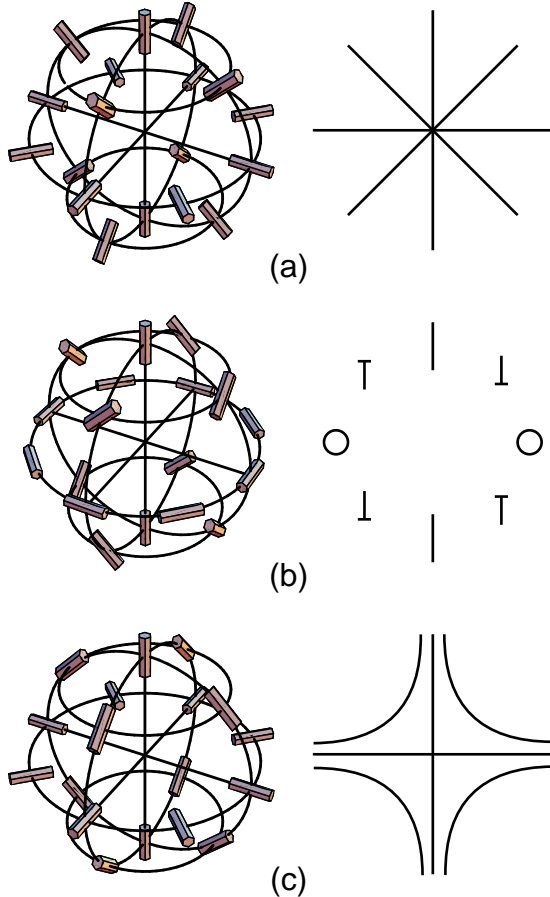


FIG. 2. (a) A radial hedgehog in which the director points radially outward from a central point like the electric field of a point charge. (b) A circular hedgehog obtained from a radial hedgehog by rotating the director at every point through $\pi/2$ about the vertical axis. (c) A hyperbolic hedgehog obtained from the radial hedgehog by rotating the director at every point by π about the vertical axis. In each case, the figures at the left provide a three-dimensional depiction of the defect whereas that at the right shows a projection onto any plane containing the polar axis. In (b), standard notation in which the nail heads indicate the end of the director coming out of the plane is used.

The energies of the simple hedgehog configurations shown in Fig. 2 in a sphere of radius R with free boundary conditions at the outer surface are easily calculated from the Frank free energy [Eq. (1)]. The Frank director

for these configurations are $\mathbf{n} = (x, y, z)/r$ for the radial, $\mathbf{n} = (y, -x, z)/r$ for the circular, and $\mathbf{n} = (-x, -y, z)/r$ for the hyperbolic hedgehogs, where $\mathbf{r} = (x, y, z)$ and $r = |\mathbf{r}|$. In a spherical region of radius R , their respective energies are

$$\begin{aligned} E_{\text{radial}} &= 8\pi(K_1 - K_{24})R \\ &\rightarrow 8\pi(K - K_{24})R \\ E_{\text{circ}} &= \frac{8\pi}{15}(3K_3 + 5K_2 + 2K_1 - 5K_{24})R \\ &\rightarrow \frac{8\pi}{3}(2K - K_{24})R \\ E_{\text{hyper}} &= \frac{8\pi}{15}(3K_1 + 2K_3 + 5K_{24})R \\ &\rightarrow \frac{8\pi}{3}(K + K_{24})R, \end{aligned} \quad (8)$$

where the final expressions are for the case of equal elastic constants. When $K_{24} = 0$, these energies reduce to those calculated in Ref. [33]. The hyperbolic hedgehog has lower energy than the radial hedgehog provided $K_3 < 6K_1 - 10K_{24}$ or $K > 2K_{24}$ for single elastic constant approximation. Thus, if $K_{24} = 0$, the hyperbolic hedgehog always has the lower energy. The circular hedgehog has the most bend. Since K_3 is generally the largest elastic constant, the circular hedgehog generally has the highest energy provided K_{24} is not too large. If $K = 2K_{24}$, the energies of the three hedgehog configurations are equal (and equal to $4\pi KR$), as one could have predicted from Eq. (2), which is invariant with respect to rigid rotations of even a spatially varying \mathbf{n} when $K = 2K_{24}$. In confined geometries, the Rapini-Papoular surface energy competes with the K_{24} surface term to determine defect configurations.

In systems with vector symmetry, the combined topological charge [i.e., the charge obtained by evaluating Eq. (7) on any surface enclosing both hedgehog cores] of two hedgehogs with respective charges q_1 and q_2 is simply the sum $q_1 + q_2$. In nematics, the sign of the topological charge has no meaning, and the combined topological charge of two hedgehogs is either $|q_1 + q_2|$ or $|q_1 - q_2|$. It is impossible to tell with certainty which of these possible charges is the correct one by looking only at surfaces enclosing the individual hedgehogs.

We will be primarily interested in how two unit-charge hedgehogs can combine to give a hedgehog charge of zero. Figure 3 shows how a radial and a hyperbolic hedgehog can combine to give a charge-zero configuration, i.e., a configuration in which the director is parallel at infinity.

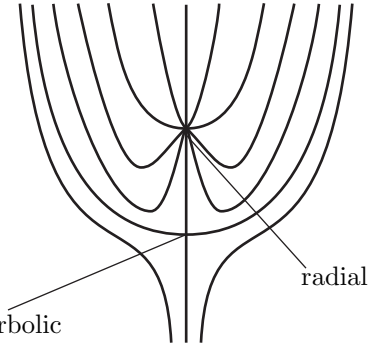


FIG. 3. A radial and a hyperbolic hedgehog combining to give a configuration with hedgehog charge zero

Disclination rings can carry a hedgehog charge q as measured by the integral in Eq. (7) evaluated over a surface enclosing the ring [47,48]. Figure 4 depicts disclination rings with far-field director configurations corresponding to radial and hyperbolic charge 1 hedgehogs. These rings can be shrunk to a point leaving a point hedgehog. Since the disclination ring is topologically equivalent to a hedgehog, one can ask whether it is energetically favorable for a point hedgehog to open up to a disclination ring [49,35]. If one assumes that order parameter configurations remain uniaxial, one can obtain a crude estimate of the radius R_0 of the disclination ring using the expressions, Eq. (6) and (8), for disclination and hedgehog energies. The director configuration of a charge 1 disclination ring is essentially that of simple disclination line discussed above Eq. (6) in the vicinity of the disclination core, i.e., up to distances of order R_0 from the ring center. Beyond this radius, the director configuration is approximately that of a hedgehog (radial or hyperbolic). Thus, we can estimate the energy of a disclination ring of radius R_0 centered in a spherical region of radius R to be

$$E_{\text{ring}} \approx 2\pi R_0 \left[\frac{1}{4}\pi K \ln(R_0/r_c) + \epsilon_c \right] + 8\pi\alpha K(R - R_0), \quad (9)$$

where $\alpha = 1 - k_{24}$ for a radial hedgehog and $\alpha = (1 + k_{24})/3$ for a hyperbolic hedgehog, where $k_{24} = K_{24}/K$. Minimizing over R_0 and setting $\epsilon_c = K$, we find

$$R_0 = r_c \exp \left[\frac{16}{\pi} \left(\alpha - \frac{1}{4} - \frac{\pi}{16} \right) \right]. \quad (10)$$

Though admittedly crude, this approximation gives a result that has the same form as that calculated in Refs. [49,35,50] using a more sophisticated continuous ansatz. It has the virtue that it applies to both radial and hyperbolic far-field configurations. It predicts that the hedgehog with the lower energy far-field configuration (i.e., the one with smaller α) will have the smaller disclination-ring radius. If $k_{24} = 0$, the hyperbolic hedgehog has the lower energy with $\alpha = 1/3$ rather than $\alpha = 1$. In this case, the core of a radial hedgehog should be a ring with radius $R_0 \approx r_c e^{2.8}$, or $R_0 \approx 0.2 \mu\text{m}$ for $r_c \approx 100 \text{\AA}$. The core

of the hyperbolic hedgehog, on the other hand will be a point rather than a ring because $R_0 \approx r_c e^{-0.58} < r_c$.

If the constraint that the tensor nematic order parameter Q_{ij} be uniaxial is relaxed, then the core of a disclination can become biaxial [51] with a core radius of order the biaxial correlation length ξ_b . The energy of a disclination is still given by Eq. (10) with $r_c \sim \xi_b$ and with a core energy determined by the energy difference between the biaxial and uniaxial state rather than the energy difference between the isotropic and nematic states. A hedgehog can also develop a biaxial core with radius of order ξ_b . Because the biaxial core is characterized by a non-vanishing biaxial order parameter, its structure is not the same as that of the uniaxial disclination ring discussed above. Calculations [52] based on the Landau-de Gennes free energy for a nematic predict a biaxial core size of order $0.025 \mu\text{m}$ for MBBA. A detailed analysis of the competition between a biaxial core and a biaxial disclination ring has not been done.

It is very difficult to predict with certainty what the core structure of a hedgehog will be. If the core is a disclination ring, its radius varies exponentially with the elastic constants. If the core is biaxial, it will have a biaxial structure out to a radius of order the biaxial correlation length, which should be of order 100\AA or less. The general arguments given above would lead one to expect hyperbolic hedgehogs to have the smallest core size. In the experiments of Poulin *et al.* [22,34], all hyperbolic hedgehogs that were observed have cores that are point-like to the resolution of the optical microscope.

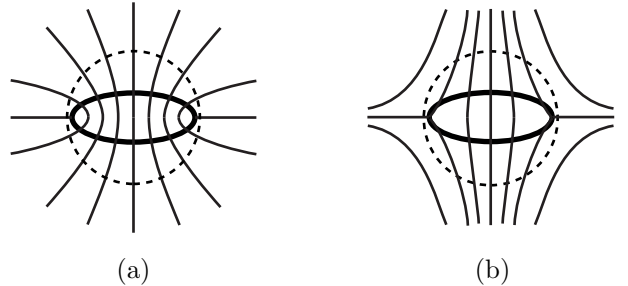


FIG. 4. Disclination rings with unit hedgehog charge: (a) radial hedgehog and (b) hyperbolic hedgehog. The dotted line in each figure represents a sphere of radius R beyond which the director configuration is that of a hedgehog.

III. DIRECTOR CONFIGURATIONS IN INVERTED NEMATIC EMULSIONS

In the experiments reported by Poulin, *et al.* [22], a nematic liquid crystal (pentyl cyano biphenyl, or 5CB), a surfactant (sodium dodecyl sulfate, SDS) and water are mixed together to produce inverted and multiple liquid crystalline emulsions. The inverted emulsions are placed in a thin rectangular cell of approximate dimensions $20 \mu\text{m} \times 1 \text{cm} \times 1 \text{cm}$. The large-area upper and lower surfaces were treated to produce tangential bound-

ary conditions. Thus, the total hedgehog charge Q in the cell, obtained by performing the integral in Eq. (7) is zero. With normal boundary conditions, each water droplet nucleates a radial hedgehog of charge one. To maintain zero charge in the cell, compensating director distortions, usually point or line defects, must be created out of the nematic itself. Possible director configurations of a single droplet with total charge zero are shown in Fig. 5. A single droplet could nucleate a companion hyperbolic hedgehog (Fig. 5a), or it could nucleate a disclination ring of finite radius lying above or below the droplet (Fig. 5b) or encircling the droplet in a “Saturn-ring” configuration (Fig. 5c). Director configurations for many droplets can be constructed from the single director configurations shown in Fig. 2. Other configurations in which the hedgehog charge of water droplets is canceled by continuous textures in the surrounding nematic rather than by the formation of point hedgehogs or singular disclination rings are possible. For example, if there are two droplets, the radial configuration around one droplet could continuously deform to a hyperbolic configuration passing through intermediate configurations such as the “circular” hedgehog of in Fig. 2b. The final hyperbolic configuration could combine with the radial configuration of the neighboring droplet to produce a configuration with zero charge but without any point defects in the nematic as shown in Fig. 6a. Alternatively, there could be a more symmetric configuration with a toroidal “escaped strength one” non-topological disclination line [53] as shown in Fig. 6b.

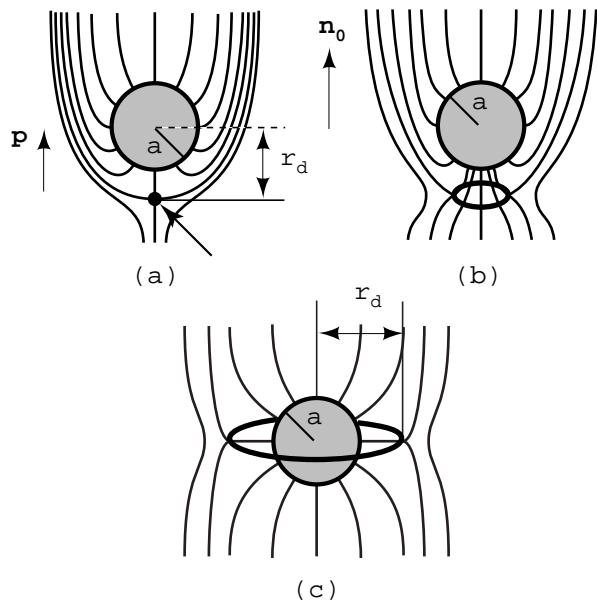


FIG. 5. Possible director configurations induced by a single spherical droplet with homeotropic boundary conditions in a nematic with total topological charge of zero. (a) Dipole configuration with a companion hyperbolic hedgehog (indicated by an arrow). (b) Dipole configuration with a companion hyperbolic disclination ring. (c) Quadrupolar saturn ring configuration with a disclination ring encircling the water droplet at its equator. The direction of the topological dipole \mathbf{p} is shown in (a).

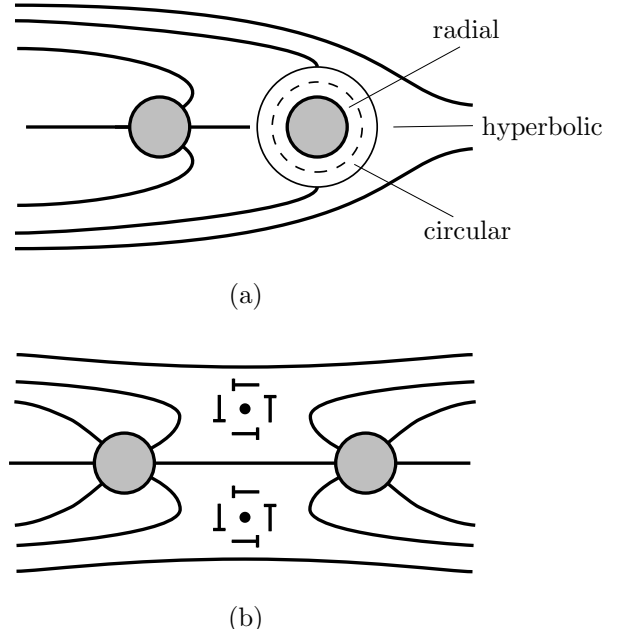


FIG. 6. Schematic representation of the nonsingular director configuration produced by two water droplets whose boundary conditions produce radial hedgehogs. (a) The radial hedgehog around one droplet converts continuously to a hyperbolic configuration which then combines with the radial configuration of the other droplet. (b) The radial configuration around each droplet converts smoothly to a toroidal “escaped strength one” non-topological disclination that encircles the axis defined by the droplets. We are grateful to R.B. Meyer for suggesting configuration (b) to us.

In the experiments of Poulin *et al.* [22,34], the dipole configuration shown in Fig. 5a is almost always observed. When many droplets are in the cell, each droplet forms a dipole with a companion hyperbolic defect so the total charge of the multiple droplet system is zero as required. Furthermore, the droplet-dipoles align in chains parallel to the cell-director as shown schematically in Fig. 7 (See also Figs. 8 and 9 of Ref. [34]). Occasionally, droplet pairs are observed to induce director configurations that cannot be interpreted in terms of companion hedgehog defects [See Fig. 12 of Ref. [34]]. These configurations may be of the type shown in Fig. 6b.

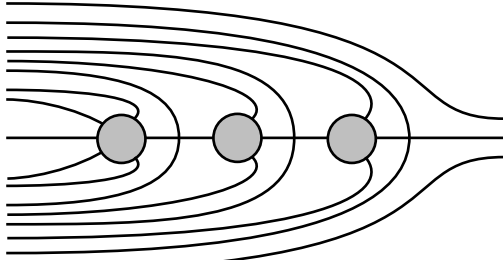


FIG. 7. Schematic representation of a chain of three water droplets in a cell with parallel boundary conditions at infinity. Each droplet creates a companion hyperbolic hedgehog, and droplets and companions defects lie on a single line.

In multiple emulsions, water droplets are confined to the interior of nematic drops with spherical symmetry. If the outer surface of the nematic drop enforces homeotropic boundary conditions, then the total topological charge in the nematic drop is one. If there are no water droplets in the nematic drop, there must be a point hedgehog defect in the interior of the drop. In general, the radial hedgehog favored by homeotropic boundary conditions at the outer surface does not have the lowest energy. Instead, there is an evolution away from the radial configuration with distance from the droplet surface [54,33], as depicted in Fig. 8a. Under crossed polarizers, this configuration will appear as rotating cross. A single water droplet in the interior of the nematic drop will create a radial hedgehog. Since the total topological charge of the nematic drop is one, no compensating defects must be created from the nematic. The configurations enforced at the water droplet surface and at the outer surface of the nematic drop are both radial. As a result, the director adopts a radial configuration throughout the drop as depicted in Fig. 8b (See Fig. 13 of Ref. [34]). Under crossed polarizers, this configuration will appear as a rigid unrotated cross. A second droplet added to a nematic drop creates an additional interior radial hedgehog. In order to satisfy the global boundary condition of charge one, a hyperbolic defect is created out of the nematic. If there are N water droplets inside a nematic drop, $N - 1$ hyperbolic defects will be created. The droplets and defects form linear chains with an unpaired droplet as shown in Fig. 9 (See also Fig. 14 of Ref. [34]). These chains (or the single water droplet if that is all there is) are rigidly placed at the center of the nematic droplet and undergo no observable Brownian motion.

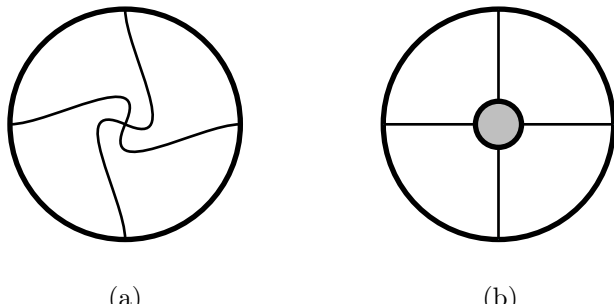


FIG. 8. (a) Schematic representation of the director configuration of a nematic drop with no interior water droplet. The director is forced by boundary conditions to have a radial configuration at the out surface. As distance from the surface increases, the director seeks lower energy, nonradial configurations. (b) Schematic representation of the director configuration of a nematic drop with a single interior water droplet. Homeotropic boundary conditions at the outer and water-droplet surfaces force a radial configuration everywhere.

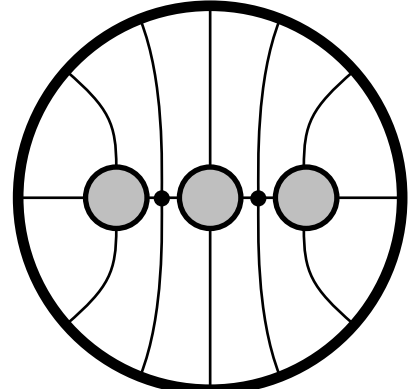


FIG. 9. A nematic drop with 3 internal water droplets. The 3 water droplets and their 2 companion hyperbolic defects form a linear chain at the center of the nematic drop. The total charge of this configuration is one.

IV. CONFIGURATION AND ENERGY OF SINGLE DROPLET

In the preceding section, we discussed possible director configurations induced by the presence of spherical water droplets with homeotropic boundary conditions in a nematic with parallel boundary conditions at infinity. Experiments show that the water droplets create companion hyperbolic hedgehogs rather than disclination rings. In this section, our goal is to calculate the equilibrium separation of the droplet from its companion and to compare the energy of the dipole configuration with that of the saturn ring and intermediate configurations depicted in Fig. 5. The calculational program is in principle quite simple: solve the Euler-Lagrange equations for the director arising from the minimization of the Frank free energy [Eq. (2)] subject to the normal boundary conditions at the surface of the water droplet and parallel boundary conditions at infinity. Unfortunately, the Euler-Lagrange equations are highly nonlinear, and analytical solutions cannot be found except for a few special geometries and boundary conditions. We can, however, obtain analytical solutions for the director far from the droplet. Using these solutions and information, evident from Fig. 5, about the form of director configurations near the droplet, we can construct variational ansatzes for the director that obey all boundary conditions and that have the desired defect structure. In this section,

we will first discuss the nature of the far-field solutions. We will then use two different ansatzes to calculate director configurations and their associated energies. The first ansatz applies only to the dipolar configuration. The second applies to all of the configurations in Fig. 5 and will allow us to compare, for example, the energies of the dipolar and Saturn-ring configurations.

A. Far-field Solutions

The constraint of zero topological charge requires $\mathbf{n}(\mathbf{r})$ to approach $\mathbf{n}_0 = (0, 0, 1)$ as $r \rightarrow \infty$. We assume that \mathbf{n}_0 is along the positive z axis. No physical results will change, however, if we reflect \mathbf{n}_0 to be along the negative z axis. At large but not infinite r , the deviation of $\mathbf{n}(\mathbf{r})$ from \mathbf{n}_0 is small, and $\mathbf{n}(\mathbf{r}) \approx (n_x, n_y, 1)$. Thus, at large r , we can replace the full nonlinear Frank free energy by the harmonic free energy

$$F_{\text{har}} = \frac{1}{2}K \sum_{\mu=x,y} \int d^3r (\nabla n_\mu)^2, \quad (11)$$

where we introduced the notation n_μ , $\mu = x, y$ for the components of \mathbf{n} perpendicular to \mathbf{n}_0 . The Euler-Lagrange equations arising from this equation are simply Laplace equations:

$$\nabla^2 n_\mu = 0. \quad (12)$$

At large r the solutions to this equation can be expanded in multipoles:

$$n_\mu = \frac{A^\mu}{r} + \frac{\mathbf{p}^\mu \cdot \mathbf{r}}{r^3} + \frac{c_{ij}^\mu r_i r_j}{r^5} + \dots \quad (13)$$

The solutions we seek are invariant with respect to rotations about the z axis and have no azimuthal component to \mathbf{n} (i.e., no twist in \mathbf{n} about the z axis). This implies that $A^\mu = 0$ and that n_x and n_y must be proportional, respectively, to x and y . In addition, the dipolar part should change sign if the position of the companion defect is shifted from above to below the droplet. The requirements are met by setting $\mathbf{p}^\mu = (\mathbf{p} \cdot \mathbf{n}_0)\mathbf{e}^\mu$ and $c_{ij}^\mu = c(n_0 i e_j^\mu + e_i^\mu n_0 j)$ where $e_i^\mu = \delta_i^\mu$ is the unit vector pointing in the $\mu = x, y$ direction. We identify the vector \mathbf{p} as the dipole moment of the droplet-defect configuration, and $\mathbf{p} \cdot \mathbf{n}_0$ with its z component. Thus if \mathbf{p} changes sign relative to \mathbf{n}_0 , the dipole contribution to n_μ also changes sign. In the configurations we consider in this section, \mathbf{p} is aligned either parallel or anti-parallel to \mathbf{n}_0 so that $\mathbf{p} \cdot \mathbf{n}_0 = \pm p$ where p is the magnitude of the dipole moment. The parameter c , as we will show in more detail in the next section, is the amplitude of the quadrupole moment tensor c_{ij} of the droplet-defect combination. Thus, we have

$$\begin{aligned} n_x &= p_z \frac{x}{r^3} + 2c \frac{zx}{r^5} \\ n_y &= p_z \frac{y}{r^3} + 2c \frac{zy}{r^5}. \end{aligned} \quad (14)$$

By dimensional analysis, $p_z \sim a^2$ and $c \sim a^3$, where a is the radius of the sphere. Equations 14 produce the far-field configurations of Fig. 5a if we choose p_z to be positive when the companion hedgehog is below the droplet. Thus, we adopt the convention that the dipole moment of the droplet and its companion defect points from the companion to the droplet.

The multipole expansion of Eqs. (13) and (14) eventually breaks down because of nonlinearities neglected in Eq. (11). We can determine the leading corrections by including the leading anharmonic corrections to the harmonic free energy. Far from the defect, we can set $\mathbf{n} = (n_x, n_y, \sqrt{1 - n_\perp^2}) \approx (n_x, n_y, 1 - \frac{1}{2}n_\perp^2)$, where $n_\perp^2 = n_\mu n_\mu$. The leading anharmonic correction to F_{har} is then

$$F_{\text{an}} = \frac{1}{8}K \int d^3r (\nabla n_\perp^2)^2, \quad (15)$$

and the Euler-Lagrange equations with this correction are

$$\nabla^2 n_\mu + \frac{1}{2}n_\mu \nabla^2 n_\perp^2 = 0. \quad (16)$$

Using this equation, one can show that if the leading contribution to n_μ is dipolar, then the first correction to n_μ arising from nonlinear terms is of the form r_μ/r^7 . In other words the multipole expansion of the Laplacian operator gives the correct large r behavior up to order r^{-5} . Thus, we could in principle develop variational approximations in which all of the multipole moments from order 2 to order 5 are variational parameters. We will content ourselves with allowing only the dipole and quadrupole moments to vary.

B. The Electric-Field Ansatz

Any ansatz for \mathbf{n} for the dipole configuration of Fig. 5a must be normal to the water droplets at $r = a$, tend to \mathbf{n}_0 as $r \rightarrow \infty$, and have a hyperbolic hedgehog at some position along the z axis outside of the water droplet. The familiar electrostatics problem of a charged conducting sphere in an external electric field can provide the basis for an ansatz for \mathbf{n} that satisfies all of these conditions. The electric field \mathbf{E} is normal to the conducting sphere, and it tends to a constant $\mathbf{E}_0 = E_0 \mathbf{e}_z$ as $r \rightarrow \infty$. If the charge Q on the sphere is large enough, there is a point below the sphere at which the electric field vanishes. The normalized electric field configuration in the vicinity of this point is identical to that of a unit vector in the vicinity of a hyperbolic hedgehog. Thus, we have all of the ingredients we need for a variational ansatz. We have merely to choose

$$\mathbf{n}(\mathbf{r}) = \mathbf{E}(\mathbf{r})/|\mathbf{E}(\mathbf{r})|. \quad (17)$$

The electric field for the above problem is

$$\frac{\mathbf{E}(\mathbf{r})}{E_0} = \mathbf{e}_z + \lambda^2 a^2 \frac{\mathbf{r}}{r^3} - \frac{a^3}{r^5} (r^2 \mathbf{e}_z - 3z\mathbf{r}), \quad (18)$$

where $\lambda^2 = Q/(E_0 a^2)$ is a unitless measure of the strength of the electric field produced by the charge Q compared to the fixed external field E_0 and a is again the radius of the sphere. The last term in this expression arises from an image dipole at the center of the sphere that enforces the boundary condition that \mathbf{E} be normal to the surface of the sphere at $r = a$. For $\lambda^2 > 3$, we find precisely one zero of the electric field at $\mathbf{r} = -z_0 \mathbf{e}_z$ outside the sphere, where z_0 is the appropriate solution to

$$|z|^3 - |z|\lambda^2 a^2 + 2a^2 = 0. \quad (19)$$

(For $\lambda^2 = 3$, the point of zero electric field just touches the sphere, and for $\lambda^2 < 3$, a singular ring appears on the surface of the sphere.) z_0 is the distance r_d from the droplet center to its companion defect. At large r , $\mathbf{n}(\mathbf{r})$ becomes

$$n_\mu = (\lambda a)^2 \frac{r_\mu}{r^3} + 3a^3 \frac{zr_\mu}{r^5} \quad (20)$$

in agreement with Eq. (14). Thus the dipole moment is $\lambda^2 a^2$ and the quadrupole moment is $3a^3/2$. The variable λ is a variational parameter that determines both the position of the hyperbolic defect and the magnitude of the dipole moment. The ansatz fixes the quadrupole moment independent of the value of λ and constrains the dipole moment to be greater than $3a^2$. A natural energy scale is $U_0 = \pi K a/2$. The reduced energy U/U_0 calculated from Eqs. (17), (18), and (1) is plotted as a function of the distance between the sphere and the companion defect in Fig. 10. The energy at the minimum of the curve is $U = 9.00U_0$. At this minimum, the other parameters characterizing the droplet-defect pair are $z_0 = 1.19a$, $p_z = 3.02a^2$, and $c = 3a^2/2$.

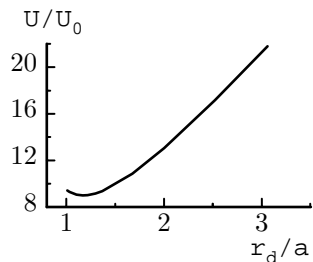


FIG. 10. Energy (in units of $U_0 = \pi K a/2$) of droplet dipole as a function of the distance (in units of the droplet radius a) from the droplet center to the companion hedgehog.

Of course we have no a priori reason to expect a normalized electric field to yield the true minimum energy configuration for this problem. By modifying our chosen $\mathbf{E}(\mathbf{r})$ to be a slightly more general vector field and by no longer insisting that it be a true electric field, we may hope to improve our ansatz and to relax the constraints put upon p_z and c . We introduce below one such

generalization that provides a significant improvement: $U = 7.87U_0$, $z_0 = 1.26a$, $p_z = 2.20a^2$, $c = -1.09a^3$. In particular, we note here that the sign of c is the opposite of what we had previously constrained it to be through our electric field ansatz.

We now present the generalization of the electric field ansatz $\mathbf{E}(\mathbf{r})$ in Eq. (18) used to calculate the the results discussed above and mention a few of the important properties it possesses. We insist that the generalization maintain the correct far-field behavior to quadrupole order so that we can identify the quadrupole strength c , as well as the dipole strength p_z . We would also like the generalization to put fewer constraints on the allowed values of p_z and c . In particular, since in certain situations the sign of c seems to be an important quantity we should certainly not restrict c to be of a particular sign in the ansatz. Rewriting Eq. (18) as,

$$\frac{\mathbf{E}(\mathbf{r})}{E_0} = \left(1 - \frac{a^3}{r^3}\right) \mathbf{e}_z + \lambda^2 a^2 \frac{\mathbf{r}}{r^3} + \frac{3za^3}{r^5} \mathbf{r} \quad (21)$$

motivates the following generalization containing the aforementioned desired properties,

$$\frac{\mathbf{E}(\mathbf{r})}{E_0} = \left(1 - \frac{a^{k_1}}{r^{k_1}}\right) \mathbf{e}_z + \lambda^2 a^2 \frac{\mathbf{r}}{r^3} + \left(\frac{\beta_1 a^3}{r^5} + \frac{\beta_2 a^{k_2}}{r^{k_2+2}}\right) z\mathbf{r}. \quad (22)$$

As before $p_z = \lambda^2 a^2$ and now $c = \beta_1 a^3/2$, provided that in carrying out the minimization over the appropriate free parameters we find k_1 and k_2 are both greater than 3 (if this had not been the case then the far-field behavior would not have been correct). Minimizing we find an energy considerably lower than that found using Eq. (18). We obtain the results for U , z_0 , p_z and C given above. In addition, we find $k_1 = 4.88$, $k_2 = 3.73$, $\beta_2 = 4.27$.

C. A Second Dipole Ansatz

To study the transition from a dipole to a Saturn ring and to establish that the dipole has a lower energy than the Saturn ring, we need an ansatz that allows disclination rings and a limiting hyperbolic hedgehog. To construct our ansatz we use appropriately symmetric solutions to a related 2D problem and modify their far-field behavior to match the required 3D far-field behavior (following a route analogous to that in [35,36] for the case of the equatorial ring).

To make contact with 2D configurations, it is convenient to look at the general problem via the following parameterization,

$$\begin{aligned} \mathbf{n} &= (\sin \Theta(\mathbf{r}) \cos \Phi(\mathbf{r}), \sin \Theta(\mathbf{r}) \sin \Phi(\mathbf{r}), \cos \Theta(\mathbf{r})) \\ \mathbf{r} &= (r \sin \theta \cos \phi, r \sin \theta \sin \phi, r \cos \theta) \end{aligned} \quad (23)$$

where we have expressed \mathbf{r} in the usual spherical coordinates. The full Euler-Lagrange equations in Θ, Φ arising from the free energy of Eq. (2) are simply,

$$\begin{aligned}\nabla^2\Theta - \sin\Theta \cos\Theta (\nabla\Phi \cdot \nabla\Phi) &= 0 \\ \sin\Theta \nabla^2\Phi + 2\cos\Theta (\nabla\Theta \cdot \nabla\Phi) &= 0\end{aligned}$$

The nonlinearity of the above coupled partial differential equations (PDE's) make closed-form solutions difficult to obtain, though we note here for completeness that $\Theta = \theta, \Phi = \phi$ is indeed a solution (the radial hedgehog) and thus that solutions are not impossible to find.

Turning now to the problem at hand, we should certainly impose the condition of azimuthal symmetry, namely: $\partial_\phi\Theta = 0, \partial_\phi\Phi = 1$, and $\Theta|_{\theta=0,\pi}$ is either 0 or π . We will impose a more stringent constraint on Φ , namely that $\Phi = \phi$, which allows us to use our knowledge of 2D nematic configurations to construct 3D azimuthally symmetric configurations (this more stringent condition was also satisfied in the electric field ansatz). This leaves us with the single Euler-Lagrange equation,

$$\nabla^2\Theta - \frac{\sin 2\Theta}{2r^2 \sin 2\theta} = 0, \quad (24)$$

whose nonlinearity still makes solutions difficult to obtain. Using now that we want $\mathbf{n} \rightarrow (0, 0, 1)$ (or $\Theta \rightarrow 0$) as $r \rightarrow \infty$, we can linearize (24) and find the form of the far-field solutions,

$$\begin{aligned}\Theta &\rightarrow \sum_{k=1}^{\infty} \frac{A_k}{r^{k+1}} P_k^1(\cos\theta) \\ &= A_1 \frac{\sin\theta}{r^2} + A_2 \frac{3\sin 2\theta}{2r^3} + \dots \\ &\equiv p_z \frac{\sin\theta}{r^2} + c \frac{\sin 2\theta}{r^3} + \dots, \quad (25)\end{aligned}$$

where the last line defines p_z and c to match the definitions of these quantities in Eq. (14), as one can check by substituting this form for Θ into Eq.(23).

Given the restriction, $\Phi = \phi$, we note that in the $x - z$ plane we have,

$$\mathbf{n}_{2D} = (\sin\Theta, \cos\Theta). \quad (26)$$

For \mathbf{n}_{2D} , we have a wealth of information about how to construct solutions for the harmonic free energy,

$$F_{2D} = \frac{1}{2}K \int d^2r (\nabla_{2D}\Theta)^2. \quad (27)$$

It would be nice if our problem reduced to this linear problem. However, even though this is not the case we can still exploit our knowledge of the 2D solutions to construct ansatz solutions for the 3D problem. The procedure is quite simple and has at least some promising motivations. Any configuration of \mathbf{n}_{2D} that is invariant under $x \rightarrow -x$ can be converted to a 3D configuration by spinning about the z axis to produce

$$\mathbf{n} = (\sin\Theta \cos\phi, \sin\Theta \sin\phi, \cos\Theta), \quad (28)$$

a solution with the $\Phi = \phi$ constraint.

Furthermore we note that the canonical $q_{2D} = +1$ defect on the z -axis becomes a $q = 1$ radial hedgehog in 3D, and the canonical $q_{2D} = -1$ defect on the z -axis becomes a $q = 1$ hyperbolic hedgehog in 3D (recall that in 2D the charges of nematic defects are signed and their composition law is addition). Also, any symmetric pair (we need a pair to maintain the required reflection symmetry about the z -axis) of $q_{2D} = \pm\frac{1}{2}$ defects off the z -axis, when spun into a 3D configuration become a strength $\frac{1}{2}$ -disclination ring. Finally, we note that satisfying the 3D BC on the sphere, namely that $\mathbf{n} = \mathbf{e}_r$ on the sphere, simply requires satisfying normal BC on the circle in 2D. In 2D we can satisfy these BC using the method of images, which works because of the linearity of the EL equations.

Before writing down the ansatz we note that the 2D configuration $\Theta = \theta_{z_0}$, where θ_{z_0} is the polar angle measured with respect to the point z_0 on the z -axis, when made into a 3D configuration indeed satisfies the 3D Euler-Lagrange (EL) equations. In two dimensions, $\Theta_1 + \Theta_2$ is a solution to the EL equations provided both Θ_1 and Θ_2 are. However, because the 3D EL equations are nonlinear, $\Theta_1 + \Theta_2$ is in general not a solution to the 3D EL equations even if Θ_1 and Θ_2 individually are. It is this fact that prevents our ansatz configurations from being true solutions to the 3D equations.

We now construct our ansatz for a sphere at the origin with a compensating unit strength hyperbolic hedgehog. To keep equations as simple as possible, we use units in which the sphere radius is one. As discussed above, we first construct a solution to the two-dimensional problem. This is done using the fact that a defect of strength q at position $\mathbf{r}_{2D} = (x_0, z_0)$ is described by the field $\Theta = q \tan^{-1}[(z - z_0)/(x - x_0)]$. Boundary conditions at the sphere's surface and at infinity can be met by placing a strength $q = +2$ defect at the sphere's center, a -1 defect at position $(0, -r_d)$ for arbitrary r_d , and an image -1 defect inside the spheres at $(0, r_d^{-1})$ as shown in Fig. 11a. This leads to

$$\Theta_0 = 2\theta - \tan^{-1} \frac{r \sin\theta}{r \cos\theta + r_d} - \tan^{-1} \frac{rr_d \sin\theta}{rr_d \cos\theta + 1}, \quad (29)$$

where we have taken the radius of the sphere to be 1, and r_d is the distance from the defect below the sphere to the origin. While this does have the correct form near the defect at $z = -r_d$ it does not have the correct far field form for the 3D problem. In fact,

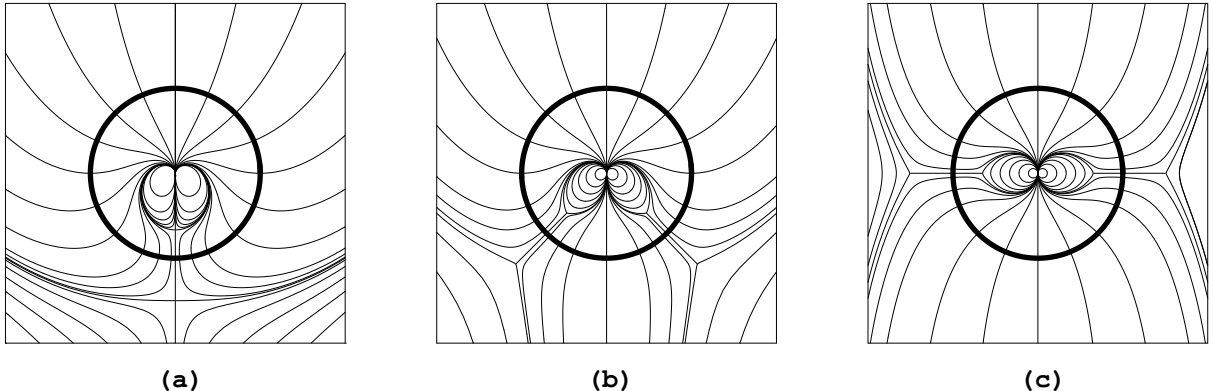


FIG. 11. Utilizing the method of images we are able to construct solutions for the related 2D problem of a nematic with homeotropic boundary conditions at infinity and with normal boundary conditions on a circle about the origin. These configurations are then extended to 3D configurations by spinning them about their vertical symmetry axis, where the singularity along the vertical axis become singularities in 3D (possibly removable ones as in the case of the +2 defect at the origin) and the symmetric pairs of defects off the axis become singular defect rings. Note that in our calculations we are not really concerned with the form of the field inside the circle since the nematic is only present in the exterior, the field is merely drawn here to elucidate the origin of the ansatz used. (a) a hyperbolic defect beneath the sphere. (b) a non-equatorial disclination ring. (c) an equatorial disclination ring.

$$\Theta_0 \approx \left(r_d + \frac{1}{r_d} \right) \frac{\sin \theta}{r} - \left(r_d^2 + \frac{1}{r_d^2} \right) \frac{\sin \theta \cos \theta}{r^2} + \dots, \quad (30)$$

which does not agree with Eq. (25). However, we note that to the order shown, it differs only by an overall power of r^{-1} (this is not true for the higher order terms not shown). So, we alter Θ_0 in the following way, taking care to preserve the BC at $r = 1$.

$$\begin{aligned} \Theta = 2\theta - \tan^{-1} \frac{r \sin \theta}{r \cos \theta + r_d} - \tan^{-1} \frac{r r_d \sin \theta}{r r_d \cos \theta + 1} \\ + e^{-k/r^3} \left[\left(r_d + \frac{1}{r_d} \right) \left(-\frac{1}{r} + \frac{1}{r^2} \right) \sin \theta \right. \\ + \frac{1}{2} \left(r_d^2 + \frac{1}{r_d^2} \right) \left(\frac{1}{r^2} - \frac{1}{r^3} \right) \sin 2\theta \\ \left. + \frac{1}{3} \left(r_d^3 + \frac{1}{r_d^3} \right) \left(-\frac{1}{r^3} + \frac{1}{r^4} \right) \sin \theta (4 \cos^2 \theta - 1) \right], \quad (31) \end{aligned}$$

which now has the far-field form,

$$\Theta \approx \left(r_d + \frac{1}{r_d} \right) \frac{\sin \theta}{r^2} - \frac{1}{2} \left(\frac{1}{r_d^2} + r_d^2 \right) \frac{\sin 2\theta}{r^3}. \quad (32)$$

This agrees with Eq. (25) with $p_z = r_d + r_d^{-1}$ and $c = -(r_d^2 + r_d^{-2})/2$, which contrary to the electric field ansatz is negative (recall $a = 1$). The factor e^{-k/r^3} , introduced for numerical convenience, tends to 1 at large r and to a value near the sphere controlled by the variational parameter k . Substituting this form [Eq. (31)] for Θ (and $\Phi = \phi$) in Eq. (2) and minimizing over r_d and k (numerically) we find, $k = 0.32$ and $r_d = 1.22$.

Now taking the sphere to have a radius of a , as in the electric-field ansatz, we find $p_z = 2.04a^2$, $c = -1.08a^3$

and $U = 7.84U_0$ in very good agreement with the results obtained from the generalized electric field ansatz. In addition $r_d = 1.22a$ agrees nicely with the corresponding quantity $z_0 = 1.26a$ obtained from the electric electric-field ansatz. Preliminary results obtained via numerical solution to the full Euler-Lagrange equations for this problem are in excellent agreement with these ansatz results [55].

D. From Dipole to Saturn Ring

We can easily generalize the angular parametrization of a point defect just discussed to describe an annular ring defect with a varying opening angle θ_d [Fig. 11b] and thereby study the transition from a dipole configuration with $\theta_d = \pi$ to the saturn ring with $\theta_d = \pi/2$ [Fig. 11c]. We proceed exactly as in the point-defect case. We place one strength +2 defect at the center of the circle, two strength $-1/2$ defects at $\mathbf{r}_{2D} = r_d(\pm \sin \theta_d, \cos \theta_d)$, and two strength $-1/2$ images inside the sphere at $\mathbf{r}_{2D} = r_d^{-1}(\pm \sin \theta_d, \cos \theta_d)$. This gives a solution to the 2D problem with two strength $-1/2$ defects outside the circle. When promoted to 3D, this solution correctly satisfies homeotropic boundary conditions at the surface of the sphere, and it yields a strength $1/2$ disclination ring outside the sphere with an opening angle of θ_d . It fails, however to produce the correct far-field form for \mathbf{n} . We add terms similar to those of the preceding calculation to correct this deficiency to produce

$$\begin{aligned} \Theta = 2\theta - \frac{1}{2} \left[\tan^{-1} \frac{r \sin \theta - r_d \sin \theta_d}{r \cos \theta - r_d \cos \theta_d} \right. \\ \left. + \tan^{-1} \frac{r \sin \theta + r_d \sin \theta_d}{r \cos \theta - r_d \cos \theta_d} \right] \end{aligned}$$

$$\begin{aligned}
& + \tan^{-1} \frac{rr_d \sin \theta - \sin \theta_d}{rr_d \cos \theta - \cos \theta_d} + \tan^{-1} \frac{rr_d \sin \theta + \sin \theta_d}{rr_d \cos \theta - \cos \theta_d} \\
& + e^{-k/r^3} \left[\left(r_d + \frac{1}{r_d} \right) \left(\frac{1}{r} - \frac{1}{r^2} \right) \cos \theta_d \sin \theta \right. \\
& + \left(r_d^2 + \frac{1}{r_d^2} \right) \left(\frac{1}{r^2} - \frac{1}{r^3} \right) (-1 + 2 \cos^2 \theta_d) \sin \theta \cos \theta \\
& + \frac{1}{3} \left(r_d^3 + \frac{1}{r_d^3} \right) \left(\frac{1}{r^3} - \frac{1}{r^4} \right) \cos \theta_d (4 \cos^2 \theta_d - 3) \times \\
& \left. \sin \theta (4 \cos^2 \theta - 1) \right]. \quad (33)
\end{aligned}$$

The director configuration in the vicinity of the disclination ring is singular, and the above form breaks down at distances from the disclination ring less than the core radius r_c . The equatorial ring configuration, $\theta_d = \pi/2$ has been investigated previously [35,36].

Figure 12 shows the energy U in units of $U_0 = \pi K a/2$ for various values of θ_d obtained by minimizing the free energy [Eq. (2)], augmented by an additional core energy $\pi r_d K \sin \theta_d/2$, over the variational parameters r_d and k in the ansatz function Eq. (33). The reduced core radius in these calculations was chosen to be $r_c = 10^{-3}$. We have checked that our results are insensitive to the value of r_c for $10^{-4} < r_c < 10^{-2}$. For a typical core radius of 10nm, or results are thus good for particles with radii as small as 1μm. Figure 13 shows the corresponding equilibrium distance of the ring from the center of the sphere. We note that r_d and E for $\theta_d \approx \pi$ agree quite well with the values obtained from the point defect ansatz previously presented. That is, this ansatz does collapse down to the point defect in a nice manner. However, we must also note that for $\theta_d = \frac{\pi}{2}$, the equatorial ring, our $r_d = 1.08a$ is somewhat different from the value of 1.25a found by Terentjev in [35,36].

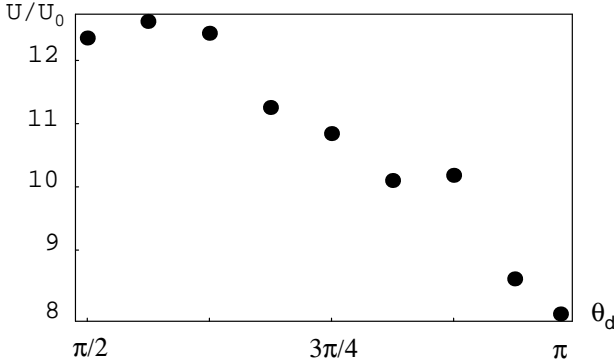


FIG. 12. Energy versus angular position of the defect ring. Note that the equatorial ring ($\theta_d = \frac{\pi}{2}$) does appear to enjoy some metastability but that the collapsed ring (or effectively the point defect, $\theta = \pi$) is of much lower energy.

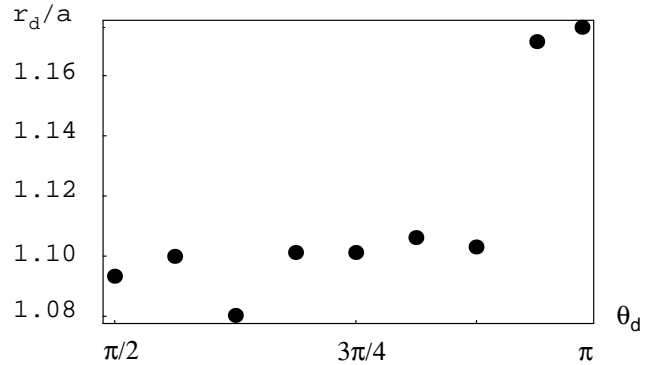


FIG. 13. The preferred distance from the origin of the disclination ring as a function of its angular position.

Further comments about the ring configuration are in order. Recalling that in three dimensions the point defect singularities represent integrable singularities whereas the ring defects do not, one might naively expect that rings should always collapse into points. As discussed in Sec. II C, however, this is not always the case. Even an isolated point singularity might have higher energy than an isolated ring singularity [49,35,50]. But it is worth noting that in such circumstances the equilibrium radius of such rings turns out to be quite small ($\approx 0.2\mu\text{m}$). Thus here we would naively expect that if a ring configuration were to exist it would probably not be an equatorial ring configuration. This proves to be correct as we see in Fig. 12. Though the equatorial ring does appear to enjoy some metastability, its energy is considerably higher than that of the point defect below the sphere.

E. Thermal Stability

We have seen so far that the point defect beneath the sphere is the energetically favorable configuration. The elastic constant k for deviations Δz from equilibrium separation z_0 is simply the curvature of the energy versus separation curve [e.g., Fig. 10]. The dipole ansatz yields $k = 33\pi K/a$. The other ansatzes yield similar values. Thus

$$\left\langle \left(\frac{\Delta z}{z_0} \right)^2 \right\rangle = \frac{k_B T}{k z_0^2} \approx 10^{-5}, \quad (34)$$

where the final numerical estimate follows from $k_B T \approx 10^{-13}\text{erg}$, $K \approx 10^{-6}\text{dyne}$, and $a = 1\mu\text{m}$. These fluctuations in the length of the topological dipole are unobservably small.

We have argued that the topological dipole prefers to align parallel or anti-parallel to the director at infinity. We will now show that the angular restoring force constant k_θ is greater than $2\pi K a$ so that

$$\langle (\Delta\theta)^2 \rangle < \frac{k_B T}{4\pi K a} \approx 10^{-4}. \quad (35)$$

Thus, though of order ten times greater than fluctuations in the length of the dipole, angular fluctuations are still unobservably small. Interestingly, we note that angular fluctuations in the 2D version of this problem are much larger and have indeed been observed in free standing smectic films [39].

Our approach is to provide an ansatz for a director configuration with the dipole rotated through an angle $\Delta\theta$ relative to the director field at infinity given a configuration in which the dipole moment is parallel to the director field at infinity. We will then use this ansatz to calculate bounds on k_θ . We start with an aligned dipole configuration with \mathbf{n} expressed in polar coordinates according to Eq. (23). We then construct a rotated configuration, \mathbf{n}' , by slowly rotating \mathbf{n} about the y -axis as we progress radially outward:

$$\begin{aligned}\mathbf{n}'_x &= \sin \Theta \cos \Phi \cos f + \cos \Theta \sin f \\ \mathbf{n}'_y &= \sin \Theta \sin \Phi \\ \mathbf{n}'_z &= \cos \Theta \cos f - \sin \Theta \cos \Phi \sin f\end{aligned}\quad (36)$$

where the amount we rotate at each point is given by the function $f(\mathbf{r})$ which must satisfy the boundary conditions,

$$\begin{aligned}f(r=a) &= 0 \\ f(r=R) &= \Delta\theta.\end{aligned}\quad (37)$$

$\Delta\theta$ denotes the tilt angle of the dipole with respect to the far-field, a the droplet radius, and R the system size. To see that $\Delta\theta$ is the stated tilt angle we note that the far-field of \mathbf{n}' makes an angle $\Delta\theta$ with the z -axis, and furthermore, the transformation of \mathbf{n} to \mathbf{n}' does not change the position of the singularity, or of the droplet itself. Thus, the droplet-defect dipole (\mathbf{p}) is still aligned with the z -axis.

We denote $F(\Delta\theta)$ as the free energy of the tilted dipole configuration and, accordingly refer to $F(0)$ as the free energy of the aligned configuration. Using Eq.(2) we find,

$$\begin{aligned}F(\Delta\theta) - F(0) &= \\ \frac{1}{2}K \int d^3r (\cos^2 \Phi \sin^2 \Theta + \cos^2 \Theta) \nabla f \cdot \nabla f\end{aligned}\quad (38)$$

where we have eliminated terms linear in f using the symmetry $F(\Delta\theta) = F(-\Delta\theta)$. Now noting that the parenthetical term is always less than unity we have,

$$F(\Delta\theta) - F(0) > \frac{1}{2}K \int d^3r \nabla f \cdot \nabla f.\quad (39)$$

The right hand side of this equation is a minimum when $\nabla^2 f = 0$ subject to the boundary conditions of Eq. (37), i.e., when

$$f = \Delta\theta \frac{1 - (a/r)}{1 - (a/R)}.\quad (40)$$

Using this f in Eq. (39), we obtain

$$F(\Delta\theta) - F(0) > 2\pi K(\Delta\theta)^2 a,\quad (41)$$

for $R \gg a$, implying $k_\theta > 4\pi K a$.

F. Optical Images

In the experiments reported by Poulin *et al.* [22], only the dipole and not the saturn ring configuration shown in Fig. 5 is observed. Figure 14a presents an experimentally obtained image of a single water droplet under crossed polarizers with one polarizer parallel to the dipole axis. In the region of the droplet we see a pronounced pattern arising from the spatially varying director field. In Fig. 14b we show an image of a similar single droplet calculated using the Jones matrix formalism [26] and neglecting any refraction at the droplet boundary. The similarity of the two images is obvious and clearly confirms the occurrence of the dipole configuration. Both pictures show two bright wings left of the droplet. In the calculated picture they are much more extended than they are in the experimental picture. The theoretical picture was calculated using the simple electric field ansatz. The more sophisticated ansatzes reduce the region around the defect where there is rapid variation of the director. They would yield images in closer agreement with the experimentally observed one.

FIG. 14. (a) Image of a single droplet with its companion defect as observed under crossed polarizers obtained by P. Poulin. (b) Simulated image of the same configuration using the Jones matrix formalism. The two images are very similar.

V. PHENOMENOLOGICAL THEORY AND DROPLET-DROPLET INTERACTIONS

To understand the properties of multi-droplet emulsions, we need to determine the nature of droplet-droplet interactions. These interactions are mediated by the nematic in which they are embedded and are in general quite complicated. Because interactions are determined by distortions of the director field, there are multi-body as well as two-body interactions. We will content ourselves with calculations of some properties of the effective two-body interaction. To calculate the position-dependent interaction potential between two droplets, we should solve the Euler-Lagrange equations, as a function of droplet separation, subject to the boundary condition that the director be normal to each droplet. Solving completely these nonlinear equations in the presence of two droplets is even more complicated than solving them with one droplet, and again we must resort to approximations. Fortunately, interactions at large separations are determined entirely by the far-field distortions and the multipole moments of the individual droplet-defect pairs, and they can be described by a phenomenological free energy, which we will derive in this section.

In the preceding section, we established that each water droplet creates a hyperbolic hedgehog to which it binds tightly to create a stable topological dipole. The original droplet is described by three translational degrees of freedom. It draws out of the nematic a hedge-

hog, which itself has three translational degrees of freedom. The two combine to produce a dipole with six degrees of freedom, which can be parametrized by three variables specifying the position of the water droplet, two angles specifying the orientation of the dipole, and one variable specifying the magnitude of the dipole. As we have seen, the magnitude of the dipole does not fluctuate much and can be regarded as a constant. The direction of the dipole is also fairly strongly constrained. It can, however, deviate from the direction of local preferred orientation (parallel to a local director to be defined in more detail below) when there are many droplets present. The droplet-defect pair is in addition characterized by its higher multipole moments. The direction of the principal axes of these moments is specified by the direction of the dipole as long as director configurations remain uniaxial. The magnitudes of the uniaxial moments like the magnitude of the dipole moment are energetically fixed. When director configurations are not uniaxial, multipole tensors will develop additional components, which we will not consider here. We can thus parametrize droplet dipoles by their position and orientation and a set of multipole moments, which we regard as fixed. Let \mathbf{e}^α be the unit vector specifying the direction of the dipole moment associated with droplet α . Its dipole and quadrupole moments are then $\mathbf{p}^\alpha = p\mathbf{e}^\alpha$ and $c_{ij}^\alpha = c(e_i^\alpha e_j^\alpha - \frac{1}{3}\delta_{ij})$, where p and c are the magnitudes of the dipole and quadrupole moments calculated in the preceding section. We can now introduce dipole- and quadrupole-moment densities, $\mathbf{P}(\mathbf{r})$ and $C_{ij}(\mathbf{r})$ in the usual way. Let \mathbf{r}^α denote the position of droplet α , then

$$\begin{aligned}\mathbf{P}(\mathbf{r}) &= \sum_\alpha \mathbf{p}^\alpha \delta(\mathbf{r} - \mathbf{r}^\alpha) \\ C_{ij}(\mathbf{r}) &= \sum_\alpha c_{ij}^\alpha \delta(\mathbf{r} - \mathbf{r}^\alpha).\end{aligned}\quad (42)$$

We now construct an effective free energy for director and droplets valid at length scales large compared to droplet dimensions. At these length scales, we can regard the droplets as point objects (as implied by the definitions of the densities given above). At each point in space, there is a local director $\mathbf{n}(\mathbf{r})$ along which the droplet-dipoles wish to align. In the more microscopic picture, of course, the direction of this local director corresponds to the far-field director \mathbf{n}_0 . The effective free energy is constructed from rotationally invariant combinations of P_i , C_{ij} , n_i , and the gradient operator ∇_i that are also even under $\mathbf{n} \rightarrow -\mathbf{n}$. It can be expressed as a sum of terms

$$F = F_{\mathbf{n}} + F_p + F_C + F_{\text{align}}, \quad (43)$$

where $F_{\mathbf{n}}$ is the Frank free energy, F_p describes interactions between \mathbf{P} and \mathbf{n} , F_C describes interactions between C_{ij} and \mathbf{n} involving gradient operators, and

$$F_{\text{align}} = -D \int d^3r C_{ij}(\mathbf{r}) n_i(\mathbf{r}) n_j(\mathbf{r})$$

$$= -DQ \sum_\alpha [(\mathbf{e}^\alpha \cdot \mathbf{n}(\mathbf{r}^\alpha))^2 - \frac{1}{3}] \quad (44)$$

describes the alignment of the axes \mathbf{e}^α along the local director $\mathbf{n}(\mathbf{r}^\alpha)$. The leading contribution to F_p is identical to that for electric dipoles in a nematic [23,56]

$$F_p = 4\pi K \int d^3r [-\mathbf{P} \cdot \mathbf{n}(\nabla \cdot \mathbf{n}) + \beta \mathbf{P} \cdot (\mathbf{n} \times \nabla \times \mathbf{n})], \quad (45)$$

where β is a material-dependent unitless parameter. The leading contribution to F_C is

$$\begin{aligned}F_C &= 4\pi K \int d^3r [(\nabla \cdot \mathbf{n}) \mathbf{n} \cdot \nabla (n_i C_{ij} n_j) \\ &\quad + \nabla (n_i C_{ij} n_j) \cdot (\mathbf{n} \times \nabla \times \mathbf{n})].\end{aligned}\quad (46)$$

There should also be terms in F_C like $C_{ij} \nabla_k n_i \nabla_k n_j$. These terms can be shown to make contributions to the effective droplet-droplet interaction that are higher order in separation than those arising from Eq. (46). Equation (46) is identical to that introduced in Ref. [37] to discuss interactions between saturn-ring droplets, provided $n_i C_{ij} n_j$ is replaced by a scalar density $\rho(\mathbf{r}) = \sum_\alpha \delta(\mathbf{r} - \mathbf{r}^\alpha)$. The two energies are absolutely equivalent to leading order in the components n_μ of \mathbf{n} perpendicular to \mathbf{n}_0 provided all \mathbf{e}^α are restricted to be parallel to \mathbf{n}_0 . When this restriction on \mathbf{e}^α is lifted, and to higher order in n_μ , the two theories differ. In our opinion, the scalar variable cannot strictly speaking be used, because each droplet carries with it an anisotropic director environment, even when the dipole moment is zero.

Since \mathbf{P} prefers to align along the local director \mathbf{n} , the dipole-bend coupling term in Eq. 45 can be neglected to leading order in deviations of the director from uniformity. The $-\mathbf{P} \cdot \mathbf{n}(\nabla \cdot \mathbf{n})$ term in Eq. (45) shows that dipoles aligned along \mathbf{n} create local splay as is evident from the dipole configuration depicted in Fig. 5a. In addition, this term says that dipoles can lower their energy by migrating to regions of maximum splay while remaining aligned with the local director. Experiments [22,34] support this conclusion. Water droplets in a nematic drop with homeotropic boundary conditions at its surface congregate at the center of the nematic drop where the splay is a maximum. Boundary conditions at the outer surface of nematic drops can be changed from homeotropic to tangential by adding a small amount of glycerol to the continuous water phase. In the passage from homeotropic to tangential boundary conditions, the topological charge of the nematic drop changes from one to zero, and point defects called boojums [30,25,31] form on the drops surface. The director splay is a maximum in the drop's interior near the boojums. Water droplets move from the drop centers to drop surfaces near boojums as the boundary conditions are changed. The final configuration of two droplets in a nematic drop with tangential boundary conditions is shown in Fig. 15.

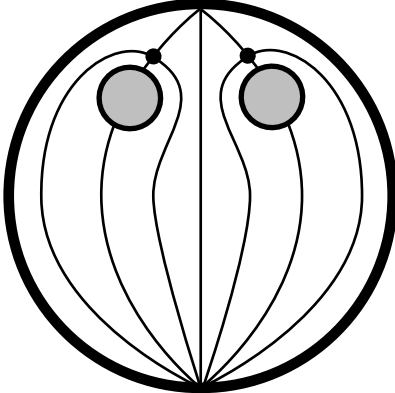


FIG. 15. Schematic representation of two water droplets with homeotropic boundary conditions at their outer surfaces in a nematic drop with tangential boundary conditions at its outer surface. The total hedgehog charge is zero, so there is one hyperbolic hedgehog per droplet. The water droplets migrate to the region of maximum splay near a surface boojum. The splay near the boojum is assumed to be sufficiently strong that both dipoles prefer to be near the boojum rather than to form a chain.

To harmonic order in n_μ , the full effective free energy is

$$F = K \int d^3r [\frac{1}{2}(\nabla n_\mu)^2 - 4\pi P_z \partial_\mu n_\mu + 4\pi(\partial_z C_{zz}) \partial_\mu n_\mu]. \quad (47)$$

The dipole-bend coupling term of Eq. (45) does not contribute because \mathbf{P} is aligned along the far-field director. Thus,

$$\nabla^2 n_\mu = 4\pi \partial_\mu [P_z(\mathbf{r}) - \partial_z C_{zz}(\mathbf{r})], \quad (48)$$

or

$$n_\mu(\mathbf{r}) = - \int d^3r' \frac{1}{|\mathbf{r} - \mathbf{r}'|} \partial'_\mu [P_z(\mathbf{r}') - \partial'_z C_{zz}(\mathbf{r}')]. \quad (49)$$

For a single droplet at the origin with $\mathbf{e} = \mathbf{n}_0$, $P_z(\mathbf{r}) = p_z \delta(\mathbf{r})$ ($p_z = \pm p$), and $C_{zz}(\mathbf{r}) = \frac{2}{3}c \delta(\mathbf{r})$, and the above equation yields exactly Eq. (14).

Droplets create far-field distortions of the director, which to leading order at large distances are determined by Eq. (48), that interact with the director fields of other droplets. This leads to an effective droplet-droplet interaction that can be expressed to leading order as pairwise interactions between dipole and quadrupole densities. Using Eq. (49) in Eq. (47), we obtain

$$\begin{aligned} \frac{F}{4\pi K} = \frac{1}{2} \int d^3r d^3r' & [P_z(\mathbf{r}) V_{PP}(\mathbf{r} - \mathbf{r}') P_z(\mathbf{r}') \\ & + C_{zz}(\mathbf{r}) V_{CC}(\mathbf{r} - \mathbf{r}') C_{zz}(\mathbf{r}') \\ & + V_{PC}(\mathbf{r} - \mathbf{r}') [C_{zz}(\mathbf{r}) P_z(\mathbf{r}') - P_z(\mathbf{r}) C_{zz}(\mathbf{r}')]] \end{aligned} \quad (50)$$

where

$$\begin{aligned} V_{PP}(\mathbf{r}) &= \partial_\mu \partial_\mu \frac{1}{r} = \frac{1}{r^3} (1 - 3 \cos^3 \theta) \\ V_{CC}(\mathbf{r}) &= -\partial_z^2 \partial_\mu \partial_\mu \frac{1}{r} = \frac{1}{r^5} (9 - 90 \cos^2 \theta + 105 \cos^4 \theta) \\ V_{PC}(\mathbf{r}) &= \partial_z \partial_\mu \partial_\mu \frac{1}{r} = \frac{\cos \theta}{r^4} (15 \cos^2 \theta - 9), \end{aligned} \quad (51)$$

where θ is the angle the separation vector \mathbf{r} makes with \mathbf{n}_0 . The interaction energy between droplets at positions \mathbf{r} and \mathbf{r}' with respective dipole and quadrupole moments p_z , p'_z , c and c' is thus

$$U(\mathbf{R}) = 4\pi K \left[p_z p'_z V_{PP}(\mathbf{R}) + \frac{4}{9} c c' V_{CC}(\mathbf{R}) \right. \\ \left. \frac{2}{3} (c p'_z - c' p_z) V_{PC}(\mathbf{R}) \right]. \quad (52)$$

This potential can be used to calculate the force between two droplets as a function of their separation. Consider, for example, the interaction between two droplets labeled 1 and 2 with respective radii a_1 and a_2 . For simplicity, assume the dipoles associated with each droplet are aligned along the positive z axis and that the center of droplet 1 is at the origin and that of droplet 2 at $\mathbf{r} = (0, 0, R)$ a distance R away along the positive z axis as shown in Fig. 16. The dipole and quadrupole moments scale respectively as a^2 and a^3 , and we can write $p_z = \alpha a^2$ and $c = -3\beta a^3/2$. The dipole ansatz solution of Sec. IVC, predicts $\alpha = 2.04$, and $\beta = (2/3) \times 1.08 = 0.72$. The force between two droplets is then

$$\begin{aligned} \frac{F}{4\pi K} = -\alpha^2 a_1^2 a_2^2 \frac{6}{R^4} + \beta^2 a_1^3 a_2^3 \frac{120}{R^6} \\ -\alpha\beta a_1^2 a_2^2 (a_1 - a_2) \frac{24}{R^5}. \end{aligned} \quad (53)$$

The dominant force is the attractive dipole-dipole force proportional to R^{-4} . Recent experiments confirm this relation [57]. Interestingly the sign of the dipole-quadrupole force, which dies off as R^{-5} , vanishes for particles of equal radius. When the particle have unequal radii, the sign of this force depends on the relative position of the large and small particle. If $a_1 < a_2$, it is repulsive (for $\beta > 0$); if $a_1 > a_2$, it is attractive, i.e., it is repulsive if the smaller ball is to the right (positive z) of the large ball and attractive if it is to the left (negative z).

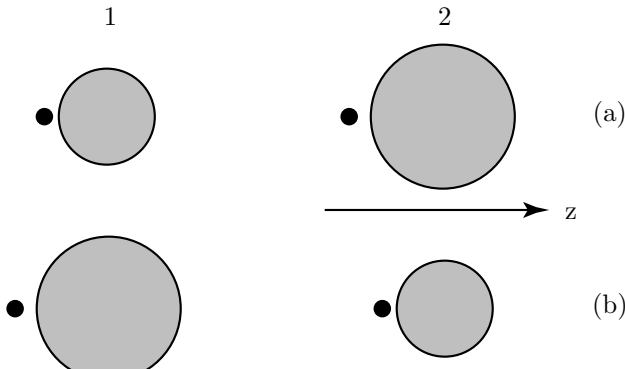


FIG. 16. (a) configuration in which the large particle is to the right of the small particle. (b) the inverse configuration. The force between the two particles is more attractive in case (a) than in case (b). In both cases, the particle to the left is labeled 1 and that to the right 2

VI. SUMMARY AND CONCLUSIONS

Inverse nematic emulsions in which surfactant coated water droplets are dispersed in a nematic host have properties that are distinct from those found in colloids, emulsions of two isotropic fluids, and of emulsions of nematic droplets in an isotropic fluid. The water droplets in these emulsions exhibit anisotropic interactions that are repulsive at short range and attractive at long range. The short-range repulsive interaction prevents coalescence of droplets and leads to long-term stability, which can be eliminated by heating into the isotropic phase. The long-range attractive force is dipolar and favors chaining of droplets.

In this paper, we have presented a detailed theoretical study of droplets and droplet interactions in inverse nematic emulsions. Homeotropic boundary conditions at droplet surfaces produce a hedgehog director configuration around each droplet. Constraints on the global topological charge force the nucleation of compensating topological defects out of the nematic host. The compensating defect associated with a single droplet in a cell with a parallel aligned director at infinity can be a point hedgehog or a disclination ring sitting above or below the droplet or encircling its equator in the saturn ring configuration as shown in Fig. 5. Using various variational ansatzes, we showed that in the lowest energy configuration, a single water droplet pulls a single point hedgehog from the nematic to form a tightly bound dipole. Then, using a phenomenological model in which the topological dipoles are coupled to the nematic director via a flexo-electric interaction, we derived the effective long-range dipolar interaction between water droplets. We also considered quadrupolar corrections to the dominant dipolar interaction. The phenomenological model also predicts the experimentally observed tendency of dipoles to seek regions of high splay.

We have focussed mostly on interactions between

droplets in cells with parallel boundary conditions at infinity with total topological charge zero. Multiple emulsions in which water droplets are dispersed in nematic drops, which are in turn dispersed in water, have made possible the isolation of a finite number of droplets and facilitated a number of experimental observations. The nematic drops are characterized by a topological charge of one rather than zero and by spatially nonuniform director configurations. Many of the properties of these droplets-within-drops systems such as chaining and the tendency of the water droplets to concentrate near the center of the nematic drop are explained by the analyses in this paper. Numerically accurate predictions about these systems, however, require, global minimization procedures that can only be done numerically. Numerical algorithms to study droplets dispersed in confined geometries are currently under development [55].

Inverse nematic emulsions are a relatively new addition to the ever growing list of interesting soft materials, and they offer the hope of new and surprising properties. We are currently investigating among other things the dynamics of droplets in inverse emulsions and inverse emulsions of water droplets in cholesteric rather than nematic liquid crystals.

ACKNOWLEDGMENTS

We are grateful for the close working relation with Philippe Poulin and David Weitz, who carried out the experiments described in this paper and without whom this work would not have been done. We are particularly grateful to Phillip Poulin for providing with Fig. 14a and to Robert Meyer for helpful discussions and for suggesting the director configuration shown in Fig. 6b. We also acknowledge helpful discussions with Arjun Yodh and Martin Zapotocky. T.C.L. and D. P. were supported primarily by the Materials Research Science and Engineering Center Program of NSF under award number DMR96-32598. H.S. Acknowledges a grant from the Deutsche Forschungsgemeinschaft under grant number Sta 352/2-2.

-
- [1] M. Kléman, *Points, Lines and Walls: in Liquid Crystals, Magnetic Systems, and Various Disordered Media* (J. Wiley, New York, 1983).
 - [2] N. Mermin, Rev. Mod. Phys. **51**, 591 (1979).
 - [3] H.-R. Trebin, Advances in Physics **31**, 195 (1982).
 - [4] P. Chaikin and T. Lubensky, *Principles of Condensed Matter Physics* (Cambridge University Press, Cambridge, 1995).
 - [5] D. Vollhardt and P. Wolfle, *The Phases of Helium 3* (Taylor and Francis, New York, 1990).

- [6] J. Wilks and D. Betts, *An Introduction to Liquid Helium* (Clarendon Press, Oxford, 1987).
- [7] G. Taylor, Proc. Roy. Soc. **145**, 362 (1934).
- [8] G. Friedel, *Dislocations* (Pergamon Press, Oxford, 1964).
- [9] F. Nabarro, *Theory of Crystal Dislocations* (Clarendon Press, Oxford, 1967).
- [10] M. Kurik and O. Lavrentovich, Sov. Phys. Usp. **31**, 196 (1988) [Usp. Fiz. Nauk. **154**, 196 (1988)].
- [11] S. Chandrasekhar and G. Ranganath, Advances in Physics **35**, 507 (1986).
- [12] *Perspectives in Quantum Hall Fluids*, edited by S. D. Sarma and A. Pinczuk (John Wiley and Sons, New York, 1997).
- [13] D. R. Nelson, in *Phase Transitions and Critical Phenomena*, edited by C. Domb and J. Lebowitz (Academic Press, New York, 1983).
- [14] K. J. Strandburg, Rev. Mod. Phys. **60**, 161 (1988).
- [15] A. Bray, Adv. Phys. **43**, 357 (1994).
- [16] A. Abrikosov, Sov. Phys. JETP **5**, 1174 (1957) [Zh. Eksp. Teor. **32**, 1442 (1957)].
- [17] G. Blatter *et al.*, Rev. Mod. Phys. **66**, 1125 (1994).
- [18] S. Renn and T. Lubensky, Phys. Rev. A **38**, 2132 (1988).
- [19] J. Goodby *et al.*, Nature **337**, 449 (1988).
- [20] J. Goodby *et al.*, J. Am. Chem. Soc **111**, 8119 (1989).
- [21] I. Chuang, R. Durrer, N. Turok, and B. Yurke, Science **251**, 1336 (1991).
- [22] P. Poulin, H. Stark, T. Lubensky, and D. Weitz, Science **275**, 1770 (1997).
- [23] R. Meyer, Phys. Rev. Lett. **22**, 918 (1969).
- [24] E. Dubois-Violette and E. Parodi, J. Physique (Paris) Colloq. **30**, C4 57 (1969).
- [25] S. Candau, P. L. Roy, and F. Debeauvais, Mol Cryst. Liq. Cryst. **23**, 283 (1973).
- [26] P. S. Drzaic, *Liquid Crystal Dispersions* (World Scientific, Singapore, 1995).
- [27] J. Doane, N. Vaz, B. Wu, and S. Žumer, Appl. Phys. Lett **48**, 269 (1986).
- [28] *Liquid Crystals in Complex Geometries*, edited by G. P. Crawford and S. Žumer (Taylor and Francis, London, 1996).
- [29] M. Kreuzer, T. Tschudi, and R. Eidenschink, Mol. Cryst. Liq. Cryst. **223**, 219 (1992).
- [30] N. Mermin, in *Quantum Fluids and Solids*, edited by S. Trickey, E. Adams, and J. Dufty (Plenum Press, New York, 1977).
- [31] M. Kurik and O. Lavrentovich, Sov. Phys. JETP Lett. **35**, 59 (1982) [Pis'ma Ah. Eksp. Teor. Fiz. **35**, 65 (1982)].
- [32] G. Volovik and O. Lavrentovich, Sov. Phys. JETP **58**, 1159 (1983) [Zh. Eksp. Teor. Fiz. **85**, 1159 (1983)].
- [33] O. Lavrentovich and E. Terentjev, Sov. Phys. JETP **64**, 1237 (1986) [Zh. Eksp. Fiz. **64**, 1237 (1986)].
- [34] P. Poulin and D. Weitz, unpublished (following paper).
- [35] E. Terentjev, Phys. Rev. E **51**, 1330 (1995).
- [36] O. Kuksenok, R. Ruhwandl, S. Shlyanovskii, and E. Terentjev, Phys. Rev. E **54**, 5198 (1996).
- [37] S. Ramaswamy, R. Nityananda, V. Raghunathan, and J. Prost, Mol. Cryst. Liq. Crystl **288**, 175 (1996).
- [38] R. Ruhwandl and E. Terentjev, Phys. Rev. E **55**, 2958 (1997).
- [39] D. Link and N. Clark, private communication.
- [40] J. Fang, E. Teer, C.M. Knobler, K.-K Loh, and J. Rudnick, to be published in Phys. Rev. E.
- [41] C. Oseen, Trans. Faraday Soc. **29**, 883 (1933).
- [42] J. Nehring and A. Saupe, J. Chem. Phys. **54**, 337 (1971).
- [43] A. Rapini and M. Papouliar, J. Phys. (Paris) **30**, (Suppl. C4), 54 (1969).
- [44] L. Blinov, A. Kabayankov, and A. Sonin, Liq. Cryst. **5**, 645 (1989).
- [45] J. H. Erdman, S. Žumer, and J. W. Doane, Phys. Rev. Lett. **64**, 1907 (1990).
- [46] T. Mason *et al.*, in *Encyclopedia of Emulsion Technology*, Vol. 4, edited by P. Becher (Marcel Dekker, Inc., New York, 1996).
- [47] A. Garel, J. Physique (Paris) **39**, 225 (1978).
- [48] H. Nakanishi, K. Hayashi, and Hiroyuki, Commun. Math. Phys **117**, 203 (1988).
- [49] H. Mori and H. Nakanishi, J. Phys. Soc. Jpn. **57**, 1281 (1988).
- [50] O. Lavrentovich and E. Terentjev, unpublished.
- [51] N. Schopohl and T. Sluckin, Phys. Rev. Lett. **22**, 2582 (1987).
- [52] E. Penzenstadler and H.-R. Trebin, J. Phys. France **50**, 1027 (1989).
- [53] R. Meyer, Phil. Mag. **27**, 405 (1973).
- [54] M. Press and A. Arrott, Phys. Rev. Lett. **33**, 403 (1974); M. Press and A. Arrott, J. de Physique, Colloque C1 **36**, C1 (1975).
- [55] H. Stark and J. Stelzer, unpublished.
- [56] P. de Gennes and J. Prost, *The Physics of Liquid Crystals*, 2nd Ed. (Clarendon Press, Oxford, 1993).
- [57] P. Poulin and D. Weitz, unpublished.

This figure "fig14a.gif" is available in "gif" format from:

<http://arXiv.org/ps/cond-mat/9707133v2>

This figure "fig14b.gif" is available in "gif" format from:

<http://arXiv.org/ps/cond-mat/9707133v2>